Temporal properties of the solid-state intracavity Raman laser using the traveling-wave method

Shuanghong Ding,[1,*] Xingyu Zhang,[2] Qingpu Wang,[2] Jun Zhang,[1] and Shumei Wang[1]
[1]*College of Photo-Electronic Information Science and Technology, Yantai University, Yantai 264005, People's Republic of China*
[2]*School of Information Science and Engineering, Shandong University, Jinan 250100, People's Republic of China*
(Received 23 August 2007; published 21 November 2007)

In this paper, traveling-wave (TW) equations of stimulated Raman scattering (SRS) process are deduced in detail with the phonon lifetime and backward Raman scattering considered. The numerical methods of second-order accuracy are deduced for TW equations of the SRS process. Spontaneous Raman scattering is simulated by including the stochastic shot-noise sources in phonon wave equations. The TW method is adopted to simulate the evolution of the fundamental laser inside actively *Q*-switched lasers, and the numerical results show periodical self-modulation of actively *Q*-switched pulses, which were also studied experimentally. The theoretical results were in good agreement with the experimental ones. The self-mode locking of intracavity Raman lasers are investigated numerically by adopting the TW method. It is found that the mode locking of the Stokes laser is due to the resonator net gain. The dependences of the mode-locking effect on the resonator length, transverse relaxation time of laser medium, and phonon lifetime of the Raman medium are studied numerically.

DOI: 10.1103/PhysRevA.76.053830 PACS number(s): 42.55.Ye, 42.60.Fc, 42.65.Dr, 42.55.Xi

I. INTRODUCTION

Trains of short pulses of simultaneous *Q* switching and mode locking are frequently observed in Raman lasers. Simultaneous *Q*-switching and mode locking is of great interest for the generation of high peak power and ultrashort pulses, and the high peak power from the simultaneously *Q*-switched and mode-locked laser is beneficial to wavelength conversion in an external nonlinear crystal [1] and the study on dynamic optical nonlinearities [2].

The short pulses generated through the stimulated Raman scattering (SRS) process fall in two categories. One is relaxation oscillation of first Stokes line observed in Raman generators with gas or liquid Raman media [3–5]. Johnson and Marburger [3] adopted radiation transfer equations to simulate the transient behavior for forward and backward stimulated scattered beams, and pulsations similar to relaxation oscillations are shown in the scattered intensities. This phenomenon was attributed to competition and coupling of scattered and pumping beams. The period of the pulsations is simply related to the gain length for the forward-scattered beam.

The other kind is self-mode locking of first Stokes line in intracavity Raman lasers, which consisted of a train of short pulses separated by the cavity round-trip time [6–11]. Self-mode-locking effects were observed in intracavity Raman lasers with both gas [6,7] and crystalline Raman media [8–11]. There were attempts to explain the self-mode locking of the intracavity Raman lasers theoretically. Band *et al.* established a theoretical model for the unidirectional ring laser based on the radiation transfer equations [6,7]. Though they obtained similar results to the experimental ones, it is not fully convincing to adopt the theory deduced for unidirectional ring lasers to explain the experimental results of bidirectional intracavity Raman lasers, furthermore, the backward Raman scattering was dropped in that theory. Recently, Spence adopted the radiation transfer equations to investigate the self-mode-locking effect in optical fiber Raman lasers, and revealed that the origin of the mode locking is due to the backward-SRS [6,7]. All these theories were deduced for the Raman lasers of specific configuration, and based on radiation transfer equations. These theories failed to explain the self-mode-locking effect of the crystalline intracavity Raman lasers, which is one of the mysterious phenomena of all solid-state Raman lasers [3–6]. Furthermore, radiation transfer equations neglect the transient behave of the SRS process, which is important for the mode-locked lasers.

Theoretical investigations of passively mode-locked laser systems have been done by two almost opposite approaches. The first way is computational, and one simulates the entire evolution of light starting from noise within the resonator [12–15]. The other one introduced by Haus [16,17] is analytical, and uses an assumption in which the pulse evolution in a single pass through laser medium is assumed to be small to obtain a simple equation analyzing the performance of the passively mode-locked lasers.

For the first approach, Fleck adopted the traveling-wave (TW) method to study the evolution of the pulse in passively mode-locked and *Q*-switched lasers [12–14]. From then on, the TW method has been considered to be one of key theoretical models of passive mode locking. In the TW method, the laser field evolution from the noise is simulated based on the direct solution of Maxwell's equations and boundary conditions imposed by laser resonator. Such a treatment avoids any explicit assumptions regarding the longitudinal mode structure of lasers, and is ideally suited to the time-domain description of pulse phenomena. TW theories have been formulated both by neglecting the coherence of the polarization (rate-equation theories) and by taking it into account (nonrate-equation theories). In order to fully describe the temporal characteristics of pulse evolution in intracavity Raman lasers, the nonrate-equation form is adopted in this paper.

In Sec. II, based on the wave equation and SRS material equations, the traveling-wave (TW) equations of the SRS process are deduced in detail with the phonon lifetime and

*Corresponding author; dingshuanghong@yahoo.com.cn

backward Raman scattering considered. The numerical methods of second-order accuracy are deduced for TW equations in Sec. III. Spontaneous Raman scattering is simulated by including the stochastic shot-noise sources in phonon wave equations.

In Sec. IV, the TW method is adopted to simulate the evolution of the fundamental light inside the actively Q-switched laser. The numerical results show that the Q-switched pulse exhibits the periodical self-modulation, and the period is equal to the round-trip time of the resonator. From the calculation results, it is found that the degree of the modulation is related to the length of the resonator and the transverse relaxation time of the laser medium. We also observed the self-modulation effect in the output of actively Q-switched lasers experimentally. The theoretical results are in good agreement with the experimental ones.

In Sec. IV, the evolutions of first Stokes line from spontaneous Raman scattering are simulated numerically by adopting the TW method, and the numerical results show self-mode-locking effect of first Stokes line. From the numerical modeling, it is found that the mechanism of the self-mode locking of intracavity Raman lasers is similar to that of passively saturable absorbers. First Stokes line intensity grow nonlinearly with the pumping beam intensity. The lucky spike of spontaneous Raman scattering emission first surpasses SRS threshold, and experiences larger Raman gain to grow rapidly into a pulse profile after going through the Raman medium back and forth. In a word, these two passive mode-locking ways realize pulse choosing by the resonator net gain. The dependences of the self-mode-locking effect on the transverse relaxation time of laser medium, resonator length, and phonon lifetime of Raman medium are investigated numerically.

II. THEORY

A. TW equations for laser medium

The complete set of TW nonrate equations, which take the coherence of the polarization into account, are listed as [14]

$$\frac{n_1}{c}\frac{\partial E_L^+}{\partial t}+\frac{\partial E_L^+}{\partial z}=-\langle \rho \exp(ikz)\rangle, \tag{1a}$$

$$\frac{n_1}{c}\frac{\partial E_L^-}{\partial t}-\frac{\partial E_L^-}{\partial z}=-\langle \rho \exp(-ikz)\rangle, \tag{1b}$$

$$\frac{\partial \rho}{\partial t}+T_{L2}^{-1}\rho=-\frac{1}{2}T_{L2}^{-1}\sigma_0 n[E_L^+\exp(-ikz)+E_L^-\exp(ikz)], \tag{1c}$$

$$\frac{\partial n}{\partial t}=T_{L1}^{-1}(n^0-n)+4[\rho E_L^{+*}\exp(ikz)+\rho E_L^{-*}\exp(-ikz)+\text{c.c.}], \tag{1d}$$

where E_L^+ and E_L^- are the normalized amplitudes of the forward and backward traveling fundamental laser, respectively. $(E_L^{\pm})^2$ is the flux of the photon density $(\text{cm}^{-2}\,\text{sec}^{-1})$. The optical electric field $E_L^{\pm}$ is assumed to propagate in the $\pm z$ directions, respectively, and k the wave number of laser field. ρ is the normalized amplitude of nonlinear polarization vector. n is the population difference variable between the upper and lower states of laser medium, and n^0 the initial value. c is light speed in the vacuum, and n_1 the refractive index of the laser medium. T_{L1} and T_{L2} are the longitudinal and transverse relaxation times of the laser medium, and σ_0 the stimulated emission cross section. Brackets in Eqs. (1a) and (1b) mean taking spatial averages of quantities, which contribute to the slowly varying optical field $E_L^{\pm}$.

B. TW equations for SRS

In the Raman media, SRS vibration mode corresponds to the most intensive spontaneous Raman scattering line, so the Raman medium can be considered as a two-level system with a_0 and a_1 representing the amplitude of the normalized wave functions of ground and excited states, respectively. For the uniform and isotropic medium, the scalar wave equation can be deduced from the Maxwell equations and written as following:

$$\frac{\partial^2 E}{\partial z^2}-\frac{n_2^2}{c^2}\frac{\partial^2 E}{\partial t^2}=\frac{4\pi}{c^2}\frac{\partial^2 P}{\partial t^2}, \tag{2}$$

where n_2 is the refractive index of the Raman medium. The optical electric field E is assumed to be the plane wave linearly polarized along the x axis, and it propagates in the $\pm z$ directions. The nonlinear polarization P vector is also assumed to be linearly polarized along the x axis.

The nonlinear polarization response of Raman media can be described by a system of material equations [18–20],

$$P=N\frac{\partial \alpha}{\partial q}QE, \tag{3a}$$

$$\frac{\partial^2 Q}{\partial t^2}+\Gamma\frac{\partial Q}{\partial t}+\omega_0^2 Q=\frac{1}{4m}\frac{\partial \alpha}{\partial q}E^2\Delta, \tag{3b}$$

$$\frac{\partial \Delta}{\partial t}=-\frac{1}{\hbar\omega_0}\left(\frac{\partial \alpha}{\partial q}\right)E^2\frac{\partial Q}{\partial t}+\Gamma'(1-\Delta), \tag{3c}$$

where $Q=\langle q'\rangle$ is the expectation value of the amplitude of the stimulated normal vibrational mode, N the molecular density, and $N\Delta=N(a_0a_0^*-a_1a_1^*)$ the population difference between the ground and excited states. $\partial\alpha/\partial q$ is the normal-mode derivative of the molecular polarizability tensor. m is the effective mass associated with the q vibration and ω_0 is the center angular frequency of the lattice vibration. The damping constant Γ corresponds to $1/T_{S2}$, and T_{S2} is the lifetime of the excited phonon. The damping constant Γ' corresponding to $1/T_{S1}$ is the inverse lifetime of the excited vibrational state.

In general, when the intensity of the pumping field is extraordinary high, Eqs. (3b) and (3c) must be solved as coupled nonlinear equations. For many stimulated Raman experiments however, negligible population transfer occurs from the ground state to the excited one, and in addition

$\omega_0 \gg kT/\hbar$. Under these situations $\Delta=1$, and the macroscopic equations describing interaction of the fields and the lattice can be written as follows [21]:

$$\frac{\partial^2 Q}{\partial t^2} + \Gamma \frac{\partial Q}{\partial t} + \omega_0^2 Q = \frac{1}{4m}\frac{\partial \alpha}{\partial q} E^2, \tag{4a}$$

$$P = N\frac{\partial \alpha}{\partial q} QE, \tag{4b}$$

$$\frac{\partial^2 E}{\partial z^2} - \frac{n_2^2}{c^2}\frac{\partial^2 E}{\partial t^2} = \frac{4\pi}{c^2}\frac{\partial^2 P}{\partial t^2}. \tag{4c}$$

By neglecting high-order Stokes and anti-Stokes waves, the paraxial solution of the wave equation (4c) can be expressed as the sum of interacting linearly polarized waves

$$E = \frac{1}{2}\{E_L^+ \exp[i(\omega_L t - k_L z)] + E_L^- \exp[i(\omega_L t + k_L z)] + E_S^+ \exp[i(\omega_S t - k_S z)] + E_S^- \exp[i(\omega_S t + k_S z)] + \text{c.c.}\}, \tag{5}$$

where $\omega_{L,S}$ is the angular frequency of the fundamental and first Stokes wave, respectively, and $k_{L,S}$ the wave number of each wave component. $E_L^{\pm}$ and $E_S^{\pm}$ are the slowly varying amplitudes of forward and backward fundamental and first Stokes waves, respectively, which fulfill the following relations

$$\left|\frac{\partial^2 E_{S,L}^{\pm}}{\partial t^2}\right| \ll \left|\omega_{S,L}\frac{\partial E_{S,L}^{\pm}}{\partial t}\right|, \quad \left|\frac{\partial^2 E_{S,L}^{\pm}}{\partial z^2}\right| \ll \left|k_{S,L}\frac{\partial E_{S,L}^{\pm}}{\partial z}\right|. \tag{6}$$

We consider here only the resonant case, i.e., $\omega_L = \omega_0 + \omega_S$. The expectation value Q of the molecular displacement has the form

$$Q = \frac{1}{2}\{q_+^+ \exp[i(\omega_0 t - k_0^+ z)] + q_+^- \exp[i(\omega_0 t + k_0^+ z)] + q_-^+ \exp[i(\omega_0 t - k_0^- z)] + q_-^- \exp[i(\omega_0 t + k_0^- z)] + \text{c.c.}\}, \tag{7}$$

where $q^{\pm}{}_{\pm}$ is the slowly varying amplitude of the phonon wave component. The phonon wave number $k_0{}^+ = k_L - k_S$ satisfies the phase matching condition of the forward SRS, and couples $E_S{}^+(E_S{}^-)$ and $E_L{}^+(E_L{}^-)$ together. $k_0{}^- = k_L + k_S$ fulfills the phase matching condition of backward SRS, and couples $E_S{}^+(E_S{}^-)$ and $E_L{}^-(E_L{}^+)$ together.

If only considering the resonant interaction of third-order nonlinearity $\chi^{(3)}$, we obtain

$$P = \frac{1}{2}(P_L^+ + P_L^- + P_S^+ + P_S^-) + \text{c.c.} \tag{8}$$

Nonlinear polarization components can be obtained by substituting Eqs. (5), (7), and (8) into Eq. (4b),

$$P_L^+ = \frac{1}{2}N\frac{\partial \alpha}{\partial q}\exp[i(\omega_L t - k_L z)](E_S^+ q_+^+ + E_S^- q_-^+), \tag{9a}$$

$$P_L^- = \frac{1}{2}N\frac{\partial \alpha}{\partial q}\exp[i(\omega_L t + k_L z)](E_S^+ q_-^- + E_S^- q_+^-), \tag{9b}$$

$$P_S^+ = \frac{1}{2}N\frac{\partial \alpha}{\partial q}\exp[i(\omega_S t - k_S z)](E_L^+ q_+^{+*} + E_L^- q_-^{-*}), \tag{9c}$$

$$P_S^- = \frac{1}{2}N\frac{\partial \alpha}{\partial q}\exp[i(\omega_S t + k_S z)](E_L^+ q_-^{+*} + E_L^- q_+^{-*}). \tag{9d}$$

By substituting Eqs. (5) and (7) into Eq. (4a), making Eqs. (5), (8), and (9) into Eq. (4c), adopting the slowly varying approximation Eq. (6), and neglecting nonresonant interactions, the coupled differential equations describing the evolution of complex amplitudes of the fundamental, first Stokes waves and phonon waves can be obtained,

$$\frac{n_2}{c}\frac{\partial E_L^+}{\partial t} + \frac{\partial E_L^+}{\partial z} = -i\frac{\pi N \omega_L}{n_2 c}\frac{\partial \alpha}{\partial q}(q_+^+ E_S^+ + q_-^+ E_S^-), \tag{10a}$$

$$\frac{n_2}{c}\frac{\partial E_L^-}{\partial t} - \frac{\partial E_L^-}{\partial z} = -i\frac{\pi N \omega_L}{n_2 c}\frac{\partial \alpha}{\partial q}(q_-^- E_S^+ + q_+^- E_S^-), \tag{10b}$$

$$\frac{n_2}{c}\frac{\partial E_S^+}{\partial t} + \frac{\partial E_S^+}{\partial z} = -i\frac{\pi N \omega_S}{n_2 c}\frac{\partial \alpha}{\partial q}(q_+^{+*} E_L^+ + q_-^{-*} E_L^-), \tag{10c}$$

$$\frac{n_2}{c}\frac{\partial E_S^-}{\partial t} - \frac{\partial E_S^-}{\partial z} = -i\frac{\pi N \omega_S}{n_2 c}\frac{\partial \alpha}{\partial q}(q_-^{+*} E_L^+ + q_+^{-*} E_L^-), \tag{10d}$$

$$\frac{\partial q_-^-}{\partial t} + \frac{\Gamma}{2}q_-^- = -i\frac{1}{4m\omega_0}\frac{\partial \alpha}{\partial q}E_L^- E_S^{+*}, \tag{10e}$$

$$\frac{\partial q_-^+}{\partial t} + \frac{\Gamma}{2}q_-^+ = -i\frac{1}{4m\omega_0}\frac{\partial \alpha}{\partial q}E_L^+ E_S^{-*}, \tag{10f}$$

$$\frac{\partial q_+^-}{\partial t} + \frac{\Gamma}{2}q_+^- = -i\frac{1}{4m\omega_0}\frac{\partial \alpha}{\partial q}E_L^- E_S^{-*}, \tag{10g}$$

$$\frac{\partial q_+^+}{\partial t} + \frac{\Gamma}{2}q_+^+ = -i\frac{1}{4m\omega_0}\frac{\partial \alpha}{\partial q}E_L^+ E_S^{+*}. \tag{10h}$$

We introduce the normalized amplitudes of laser and phonon waves,

$$E_{L,S}^{\pm} \to \sqrt{\frac{cn_2}{4\pi\hbar\omega_{S,L}}}E_{L,S}^{\pm}, \tag{11a}$$

$$Q_{\pm}^{\pm} = i\frac{\pi N\sqrt{\omega_L \omega_S}}{n_2 c}\frac{\partial \alpha}{\partial q}q_{\pm}^{\pm}. \tag{11b}$$

After being normalized, $(E_{L,S}^{\pm})^2$ is the flux of the photon density ($\text{cm}^{-2}\,\text{sec}^{-1}$).

The Raman gain coefficient at the first Stokes wavelength in the steady-state regime can be expressed as

$$g_s = \frac{8\pi^2 N\omega_S}{c^2 n_2^2 m\omega_0 \Gamma}\left(\frac{\partial\alpha}{\partial q}\right)^2. \tag{12}$$

Multiplexing two sides of Eq. (10) by $(cn_2/4\pi\hbar\omega_{S,L})^{1/2}$, and substituting Eqs. (11) and (12) into Eq. (10), normalized SRS traveling wave equations can be obtained,

$$\frac{n_2}{c}\frac{\partial E_L^+}{\partial t} + \frac{\partial E_L^+}{\partial z} = -(Q_+^+ E_S^+ + Q_-^+ E_S^-), \tag{13a}$$

$$\frac{n_2}{c}\frac{\partial E_L^-}{\partial t} - \frac{\partial E_L^-}{\partial z} = -(Q_-^- E_S^+ + Q_+^- E_S^-), \tag{13b}$$

$$\frac{n_2}{c}\frac{\partial E_S^+}{\partial t} + \frac{\partial E_S^+}{\partial z} = Q_+^{+*} E_L^+ + Q_-^{-*} E_L^-, \tag{13c}$$

$$\frac{n_2}{c}\frac{\partial E_S^-}{\partial t} - \frac{\partial E_S^-}{\partial z} = Q_-^{+*} E_L^+ + Q_+^{-*} E_L^-, \tag{13d}$$

$$\frac{\partial Q_-^-}{\partial t} + \frac{\Gamma}{2}Q_-^- = \frac{1}{4}g_s\hbar\omega_L\Gamma E_L^- E_S^{+*} + Rs_-^-, \tag{13e}$$

$$\frac{\partial Q_-^+}{\partial t} + \frac{\Gamma}{2}Q_-^+ = \frac{1}{4}g_s\hbar\omega_L\Gamma E_L^+ E_S^{-*} + Rs_-^+, \tag{13f}$$

$$\frac{\partial Q_+^-}{\partial t} + \frac{\Gamma}{2}Q_+^- = \frac{1}{4}g_s\hbar\omega_L\Gamma E_L^- E_S^{-*} + Rs_+^-, \tag{13g}$$

$$\frac{\partial Q_+^+}{\partial t} + \frac{\Gamma}{2}Q_+^+ = \frac{1}{4}g_s\hbar\omega_L\Gamma E_L^+ E_S^{+*} + Rs_+^+. \tag{13h}$$

The last term in Eqs. (13e)–(13h) is the fluctuating contributions to the phonon wave, which acts as the SRS source to Eqs. (13a)–(13d).

III. NUMERICAL METHOD FOR THE SRS TRAVELING-WAVE EQUATIONS

The Stokes and fundamental beams will be generated when bouncing back and forth within the resonator. It should be an iteration process to obtain the output of the Stokes beams taking the two resonator mirrors as the boundary. The numerical accuracy is crucial to the TW method, because tens of thousands of integration cycles are required for the general applications. In this section, the numerical methods of second-order accuracy are deduced for Eq. (13) at moderate computation expense by adopting the method of Fleck [14]. For the numerical calculations, a finite-difference grid of two dimensions t and z is adopted as shown in Fig. 1.

The ordinary differential equations in Eqs. (13e)–(13h) have the following form:

$$\frac{\partial x}{\partial t} + T^{-1}x = f. \tag{14}$$

Integrating Eq. (14) from $t_m = m\Delta t$ to $t_{m+1} = (m+1)\Delta t$, we obtain

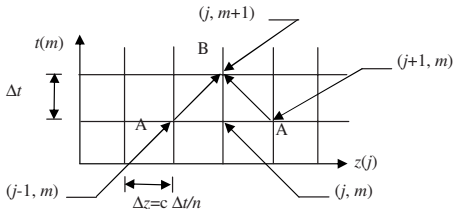

FIG. 1. Finite-difference grid for numerical solution. Arrows indicate integration paths used in reducing differential equations to finite-difference equations.

$$x_j^{m+1} = x_j^m e^{-\Delta t/T} + \int_{t_m}^{t_{m+1}} e^{-(t-t')/T} f(t')dt', \tag{15}$$

where $x_j^m = x(j\Delta z, m\Delta t)$. If $f(t')$ is assumed to vary linearly between t_m and t_{m+1}, the integral can be evaluated explicitly with

$$x_j^{m+1} = Cx_j^m + Af_j^m + Bf_j^{m+1} + O((\Delta t)^3), \tag{16}$$

where

$$f_j^m = f(j\Delta z, m\Delta t), \tag{17a}$$

$$C = e^{-\Delta t/T}, \tag{17b}$$

$$A = T[(T/\Delta t)(1 - e^{-\Delta t/T}) - e^{-\Delta t/T}], \tag{17c}$$

$$B = T[1 - (T/\Delta t)(1 - e^{-\Delta t/T})]. \tag{17d}$$

Equation (16) is the basis for creating the numerical method of Eqs. (13e)–(13h), and has second-order accuracy.

Equations (13a)–(13d) have the similar form as

$$\frac{n_2}{c}\frac{\partial y}{\partial t} \pm \frac{\partial y}{\partial t} = g. \tag{18}$$

The partial derivatives on the left-hand side of Eq. (18) can be expressed in terms of a directional derivative along the characteristic,

$$D\frac{\partial y}{\partial s} = g, \tag{19}$$

where $D = [(\eta_2/c)^2 + 1]^{1/2}$. By integrating Eq. (19) from $A \equiv ((j \mp 1)\Delta z, m\Delta t)$ to $B \equiv (j\Delta z, (m+1)\Delta t)$ along the characteristic as shown in Fig. 1, we obtain

$$y_j^{m+1} - y_{j\mp1}^m = D^{-1}\int_A^B g ds. \tag{20}$$

Assuming that g varies linearly along the characteristic between A and B, Eq. (20) becomes

$$y_j^{m+1} - y_{j\mp1}^m = \frac{1}{2}\Delta z(g_j^{m+1} + g_{j\mp1}^m) + O((\Delta z)^3). \tag{21}$$

Equation (21) provides the way to generate the numerical methods of Eqs. (13a)–(13d), and also has second-order accuracy.

By adopting Eqs. (16) and (21), the numerical methods of Eq. (13) are summarized as follows:

$$E_{Lj}^{+m+1} + \frac{1}{2}\Delta z Q_{+j}^{+m+1} E_{Sj}^{+m+1} + \frac{1}{2}\Delta z Q_{-j}^{+m+1} E_{Sj}^{-m+1} = E_{Lj-1}^{+m} - \frac{1}{2}\Delta z (Q_{+j-1}^{+m} E_{Sj-1}^{+m} + Q_{-j+1}^{+m} E_{Sj+1}^{-m}), \quad (22a)$$

$$E_{Lj}^{-m+1} + \frac{1}{2}\Delta z Q_{-j}^{-m+1} E_{Sj}^{+m+1} + \frac{1}{2}\Delta z Q_{+j}^{-m+1} E_{Sj}^{-m+1} = E_{Lj+1}^{-m} - \frac{1}{2}\Delta z (Q_{-j-1}^{-m} E_{Sj-1}^{+m} + Q_{+j+1}^{-m} E_{Sj+1}^{-m}), \quad (22b)$$

$$E_{Sj}^{+m+1} - \frac{1}{2}\Delta z Q_{+j}^{+m+1*} E_{Lj}^{+m+1} - \frac{1}{2}\Delta z Q_{-j}^{-m+1*} E_{Lj}^{-m+1} = E_{Sj-1}^{+m} + \frac{1}{2}\Delta z (Q_{+j-1}^{+m*} E_{Lj-1}^{+m} + Q_{-j+1}^{-m*} E_{Lj+1}^{-m}), \quad (22c)$$

$$E_{Sj}^{-m+1} - \frac{1}{2}\Delta z Q_{-j}^{+m+1*} E_{Lj}^{+m+1} - \frac{1}{2}\Delta z Q_{+j}^{-m+1*} E_{Lj}^{-m+1} = E_{Sj-1}^{-m} + \frac{1}{2}\Delta z (Q_{-j-1}^{+m*} E_{Lj-1}^{+m} + Q_{+j+1}^{-m*} E_{Lj+1}^{-m}), \quad (22d)$$

$$Q_{+j}^{+m+1} = CQ_{+j}^{+m} + AGE_{Lj}^{+m} E_{Sj}^{+*m} + BGE_{Lj}^{+m+1} E_{Sj}^{+*m+1} + Rs\exp(i\phi_{+m+1,j}^{+}), \quad (22e)$$

$$Q_{+j}^{-m+1} = CQ_{+j}^{-m} + AGE_{Lj}^{-m} E_{Sj}^{-*m} + BGE_{Lj}^{-m+1} E_{Sj}^{-*m+1} + Rs\exp(i\phi_{+m+1,j}^{-}), \quad (22f)$$

$$Q_{-j}^{+m+1} = CQ_{-j}^{+m} + AGE_{Lj}^{+m} E_{Sj}^{-*m} + BGE_{Lj}^{+m+1} E_{Sj}^{-*m+1} + Rs\exp(i\phi_{-m+1,j}^{+}), \quad (22g)$$

$$Q_{-j}^{-m+1} = CQ_{-j}^{-m} + AGE_{Lj}^{-m} E_{Sj}^{+*m} + BGE_{Lj}^{-m+1} E_{Sj}^{+*m+1} + Rs\exp(i\phi_{-m+1,j}^{-}), \quad (22h)$$

where

$$G = \frac{1}{4} g_s \hbar \omega_L \Gamma, \quad (23a)$$

$$C = e^{-\Delta t\Gamma/2}, \quad (23b)$$

$$A = \frac{2}{\Gamma}[(2/\Delta t\Gamma)(1 - e^{-\Delta t\Gamma/2}) - e^{-\Delta t\Gamma/2}], \quad (23c)$$

$$B = \frac{2}{\Gamma}[1 - (2/\Delta t\Gamma)(1 - e^{-\Delta t\Gamma/2})]. \quad (23d)$$

Eight implicit difference equations in Eqs. (23) are the nonlinear equations, and can be solved by the iteration method to obtain the values of E_{Lj}^{+m+1}, E_{Lj}^{-m+1}, E_{Sj}^{+m+1}, E_{Sj}^{-m+1}, Q_{+j}^{+m+1}, Q_{+j}^{-m+1}, Q_{-j}^{+m+1}, Q_{-j}^{-m+1} for $t_{m+1}=(m+1)\Delta t$ with results having been calculated. However, the iteration method is time consuming, and not convergent sometimes. In our calculation, $E_{L,Sj}^{\pm\ m+1}$ are replaced by the linearly extrapolated values $\hat{E}_{L,Sj}^{\pm\ m+1}$ from the two previous integration cycle times $E_{L,Sj}^{\pm\ m}$ and $E_{L,Sj}^{\pm\ m-1}$ when Eqs. (23e)–(23h) are solved to obtain $Q_{\pm j}^{\pm m+1}$, then substitute $Q_{\pm j}^{\pm m+1}$ into Eqs. (23a)–(23d) to obtain the values of $E_{L,Sj}^{\pm\ m+1}$. In this way, the results are always convergent, and the amount of time consumed is reduced greatly.

The spontaneous Raman scattering in Eqs. (13e)–(13h) should be Gaussian with a Lorentz spectrum, and can be written as the following form:

$$Rs_{\pm}^{\pm}(z_j,t) = Rs\sum_{m'=0}^{m} \exp(i\phi_{\pm_{m'j}}^{\pm})\delta(t - t_{m'}), \quad (24)$$

where the points are corresponding to those in a two-dimensional space-time grid, whose coordinates are $t_m = m\Delta t$ and $z_j = j\Delta z$ as shown in Fig. 1, and the phases $\phi_{\pm}^{\pm}$ are the random number between $-\pi - \pi$.

Following the way adopted by Fleck to deduce the form of the spontaneous emission source [14], the amplitude of the spontaneous Raman scattering Rs is determined,

$$Rs^2 = \frac{g\pi\Gamma^2\hbar\omega_L}{4\lambda_s^2}\left(\frac{n_2}{c}\right)^2 \Delta\Omega[1 - \exp(-\Gamma\Delta t)]. \quad (25)$$

where $\Delta\Omega$ is the solid angle subtended by E_S^+, λ_s wavelength of Stokes laser, and $\partial\sigma/\partial\Omega$ the differential scattering cross section of the Raman medium.

IV. THE NUMERICAL SIMULATION OF TEMPORAL PROPERTIES OF THE INTRACAVITY RAMAN LASER BY TW METHOD

The evolutions of fundamental and first Stokes beams are simulated numerically by adopting the TW method. In the numerical modeling, the resonator is divided into J slices, and the slice length is given by

$$dl(z) = \frac{l_C}{n(z)J}, \quad (26a)$$

$$n(z) = \begin{cases} 1, & \text{in air,} \\ n_1, & \text{in laser crystal,} \\ n_2, & \text{in Raman crystal,} \end{cases} \quad (26b)$$

where l_C is the optical length of the resonator. The time is divided into slots, whose length is

$$dt = \frac{l_C}{cn(z)J}. \quad (27)$$

Separate regions with different parameters are established for the laser medium, Raman medium, and air gap in the resonator as given in Eq. (26b). For each time slot numbered $m+1$, the coupled equations (1) are integrated within successive laser crystal slice using numerical method given in [14]; Eqs. (22) are adopted to determine the Stokes and fundamental lasers in the Raman medium; in those parts of the laser cavity where air gaps exist, the laser field is described ex-

actly by means of Eqs. (22) with the material variables disregarded. Finally, the boundary conditions at the resonator ends are taken to be the reflection conditions

$$E_{L0}^{+m+1} = -r_{L1}E_{L0}^{-m+1}, \tag{28a}$$

$$E_{S0}^{+m+1} = -r_{S1}E_{S0}^{-m+1}, \tag{28b}$$

$$E_{LJ}^{-m+1} = -r_{L2}E_{LJ}^{+m+1}, \tag{28c}$$

$$E_{SJ}^{-m+1} = -r_{S2}E_{SJ}^{+m+1}, \tag{28d}$$

where mirrors having amplitude reflection coefficients $r_{L,S1}$ and $r_{L,S2}$ are assumed to be at positions $z=0$ and $z=Jdl(z)$, J being the number of slices in the resonator. r_{L1} and r_{L2} are the reflection coefficients of the input mirror and output coupler at the pump wavelength, respectively, and r_{S1} and r_{S2} those for the Stokes beam. The above process is iterated until the output intensity of each beam is equal to zero.

Actually, $(E_{L,SJ}^{+m+1})^2[1-(r_{L,S2})^2]$ is the output photon density of fundamental and Stokes beams at the time slot numbered m+1, respectively, and the temporal profiles of the pulses can be obtained from the output photon densities of Stokes and fundamental beams.

A. Self-modulation of fundamental laser

There are reports of the periodical modulation of actively Q-switched pulses with acousto-optic (AO) [22] and electro-optic (EO) Q switches [23], and the period is equal to the round-trip transit time of the resonator. In the experiment, we observed the self-modulation of free oscillation of the flashlamp-pumped Nd:yttrium-aluminum-garnet (Nd:YAG) lasers, and the modulation of actively Q-switched pulses was also observed in the AO Q-switched laser diode (LD) end-pumped Nd:YAG laser.

In Fig. 2, the experimental oscilloscope tracings show the free oscillating output of the flashlamp-pumped Nd:YAG laser [Figs. 2(a)], and its first big spike in detail [Fig. 2(b)]. The modulation of the fundamental laser can be seen clearly in Fig. 2(b), and more detailed information is shown in Figs. 3(a) and 3(b), which are corresponding to the resonator length of 40 cm and 90 cm, respectively. In the experiment, the period of the modulation is equal to the round-trip time for most situations, however the temporal profiles of pulses exhibit some random features, e.g., a more complicated temporal profile of the self-modulated Q-switched pulse can be observed as shown in Fig. 4 with the resonator length of 90 cm. There are several peaks instead of one spike during the round-trip time in Fig. 4.

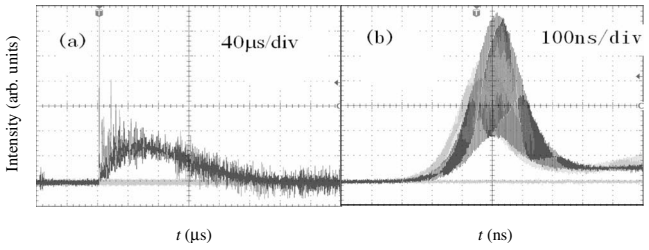

FIG. 2. Oscilloscope tracings show the free oscillating output of the flashlamp-pumped Nd:YAG laser (a), and its first big spike in detail (b).

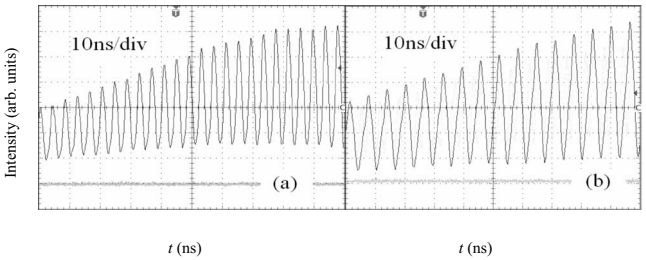

FIG. 3. Oscilloscope tracings show the first big spike of the free oscillating output from the flashlamp-pumped Nd:YAG laser in detail, and the resonator length is 40 cm (a) and 90 cm (b), respectively.

Self-modulation of pulses was also observed in the experiment of the AO Q-switched LD end-pumped Nd:YAG laser. The experimental oscilloscope tracings are shown in Figs. 5 and 6 corresponding to the resonator length of 24 cm and 45 cm, respectively, and Figs. 5(b) and 6(b) depict the detailed information. In the experiment, it is found that deeper modulation can be obtained with a longer resonator as illustrated in Figs. 5 and 6.

By using the parameters of the AO Q-switched LD end-pumped Nd:YAG laser, the TW method was adopted to simulate the evolution of actively Q-switched pulses. With active Q switch opened, large intracavity loss prohibits laser oscillation, and laser medium absorbs pumping energy to accumulate population inversion. Once the Q switch is closed, fundamental laser starts to grow from spontaneous emission radiation through the stimulated emission of inversed laser medium. Spontaneous emission radiation is the superposition of a large number of longitudinal modes with random initial phases and amplitudes. In the time domain, the spontaneous emission manifests itself as a random assortment of noise pulses of randomly varying heights and widths. Inversion population in gain medium generates polarization. By repeatedly going through the inverted gain medium, the coherence of polarization brings about temporal coherence to laser field, and individual noise spikes will begin to broaden and to smooth out. If the smoothing process is complete, active Q-switched pulses will possess perfect temporal profile, otherwise the periodical modulation can be observed in the output.

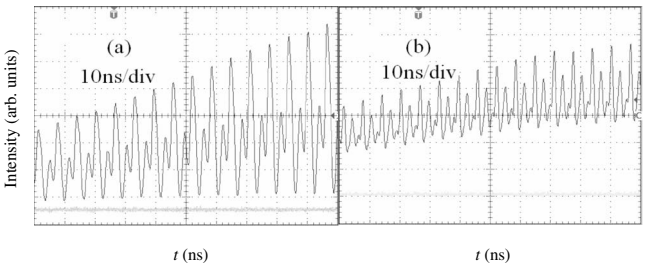

FIG. 4. Same as Fig. 3 with the resonator length of 90 cm.

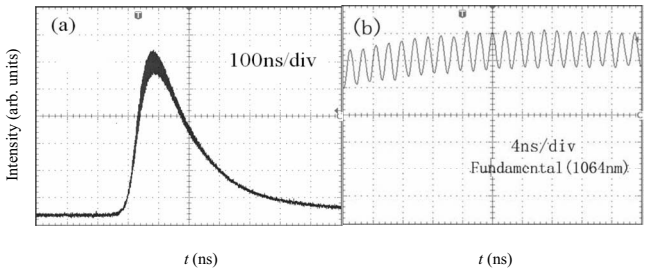

FIG. 5. Oscilloscope tracings show the pulse temporal profile from the LD end-pumped AO Q-switched Nd:YAG laser (a), and in detail (b). The resonator length are 24 cm.

The modulation depth of the actively Q-switched pulse is also related to the length of the resonator. If the round-trip time is less or nearly equal to the transverse relaxation time, the output pulse will be smoothed completely, otherwise if the round-trip time is greatly larger than the transverse relaxation time, the modulation will be generated. The numerically calculated temporal profile of the self-modulated fundamental pulse are shown in Fig. 7 for the resonator length of 45 cm, 24 cm, and 10 cm, respectively. In accordance to the experimental results, longer resonator leads to deeper modulation of the fundamental pulses. Figure 8 shows numerical results with more detail. There are statistical variations in the pulse temporal profiles from shot to shot as depicted in Fig. 8, which are due to the unavoidable statistical variations in the initial noise distribution. This phenomenon is also observed in the experiment as shown in Fig. 4.

The numerical results depicted in Fig. 9 show the influence of the transverse relaxation time on the fundamental pulse modulation. For other parameters fixed, shorter transverse relaxation time of laser media leads to lower degree of the polarization coherence, and deeper modulation can be expected.

B. Simulation of the self-mode-locking effect of first Stokes lines in intracavity Raman lasers

The TW method was adopted to numerically simulate the evolutions of the fundamental and Stokes beams for the intracavity Raman laser, and the results reveal the mode-locking effect of Stokes laser as shown in Fig. 10. Each picture represents output intensity over a single round-trip period of 3.79 ns in Fig. 10. The Stokes intensity evolution is

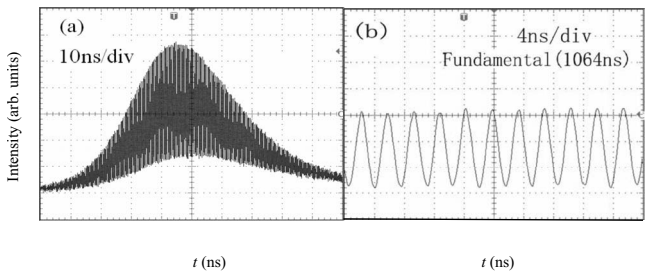

FIG. 6. Same as Fig. 5 except that the resonator length are 45 cm.

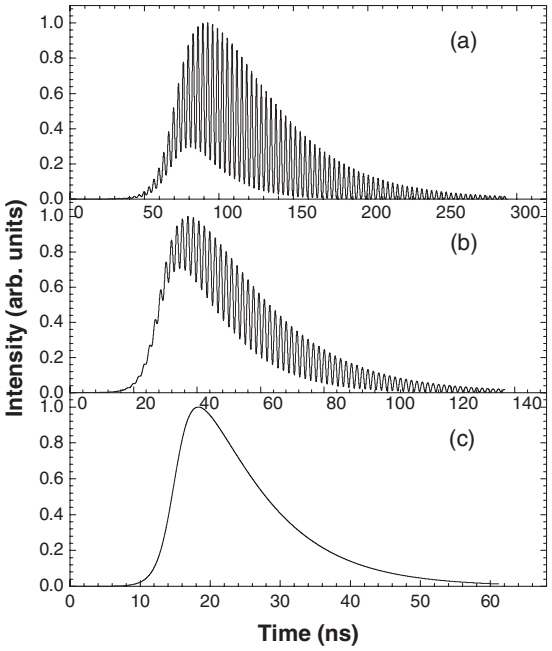

FIG. 7. Numerical results show the self-modulation of the fundamental pulses from the LD end-pumped AO Q-switched Nd:YAG laser. The resonator length is 45 cm (a), 24 cm (b), and 10 cm (c), respectively.

shown in Figs. 10(a-1)–10(a-6) with the round-trip number of 4, 14, 35, 38, 48, and 58, respectively, and the corresponding fundamental intensity evolution is shown in Figs. 10(b-1)–10(b-6). With the Q switch of the Raman laser opened, large intracavity loss prohibits the fundamental laser from oscillation, and the laser medium absorbs the pumping en-

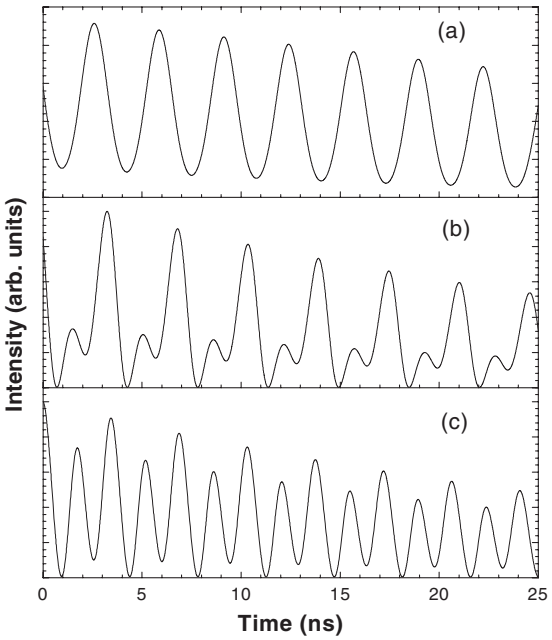

FIG. 8. Numerical results showing the detailed temporal profiles of three different outputs from the same LD end-pumped AO Q-switched Nd:YAG laser. The resonator length is 45 cm.

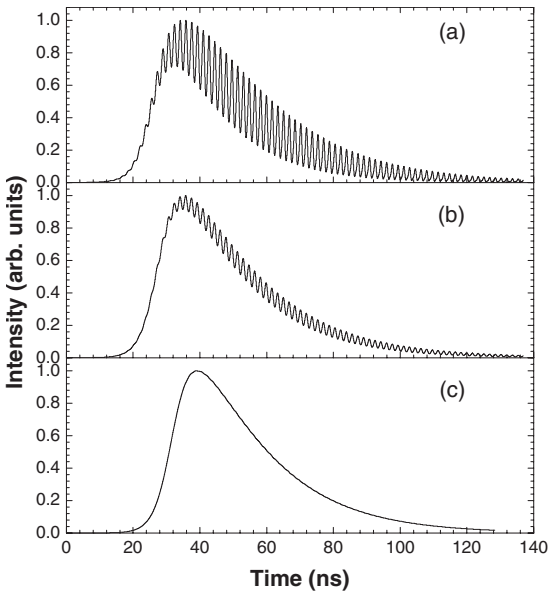

FIG. 9. Numerical results showing the influence of the transversal dephasing time on the self-modulation of the pulses from the LD end-pumped AO Q-switched Nd:YAG laser. The transveral dephasing time is $T_{L2}=1.0\times10^{-10}$ s (a), $T_{L2}=1.2\times10^{-10}$ s (b) and $T_{L2}=1.5\times10^{-10}$ s (c), respectively. The resonator length is 24 cm.

ergy to accumulate the population inversion. Once the Q switch is closed, fundamental laser starts to grow from the spontaneous emission radiation through stimulated emission of the inversed laser medium. In Fig. 10(b-1), the fundamental laser is linearly amplified, the individual noise spikes of the spontaneous emission radiation begin to be broadened. At the same time, spontaneous Raman scattering generated the weak Stokes radiation as shown in Fig. 10(a-1). The spontaneous scattering is the superposition of a large number of longitudinal modes with random initial phases and amplitudes, and manifests itself as a random assortment of initial spikes or noise pulses of randomly varying heights and widths in the time domain.

By repeatedly going through the inverted gain medium, intracavity fundamental intensity profile is smoothed out, however, there is intensity fluctuation as depicted in Figs. 10(b-2) and 10(b-3). The spontaneous Raman scattering is amplified by the SRS process by repeatedly going through the Raman medium. The individual spikes of spontaneous Raman scattering will begin to broaden and to smooth out because of the spectral narrowing caused by the finite bandpass of SRS gain as shown in Fig. 10(a-3). At the next stage, the fundamental intensity inside the resonator reaches its highest value in Fig. 10(b-4). Around the peak of the fundamental intensity, some preferred noise spike of Stokes light will first surpasses the SRS threshold. Owning to that the Stokes light grows nonlinearly with the fundamental light, the preferred spikes grow more rapidly than its less fortunate surrounding, and the Stokes output is smoothed greatly as depicted in Fig. 10(a-4). It should be noted that there is also a relative bigger spark in the right part of Fig. 10(a-4). In the nonlinearly amplifying region, the preferred pulse of Stokes laser quickly consumes the energy of the fundamental laser inside the resonator through the forward and backward SRS process, and suppresses the growth of the surrounding spikes. Thus, left-side spike eventually grow into the pulse profile with the right-side one suppressed as shown in Fig. 10(a-5). Consequently, a Q-switched burst of mode-locked pulses is generated. There is no obvious depletion of fundamental laser in Fig. 10(a-5). With rapid growth of Stokes beam, the fundamental laser is depleted quickly as shown in Fig. 10(b-6), and the left part of the fundamental laser is also depleted through the backward Raman scattering. The profile of Stokes mode-locking pulse is somewhat irregular when the Stokes beam is amplified too quickly inside the resonator.

From the numerical modeling, it is found that the mechanism of the self-mode locking of intracavity Raman lasers is similar to that of the passively saturable absorbers. For the latter, the spontaneous emission spike with the higher intensity experiences less loss when going through the saturable absorber, and eventually grows into the pulse profile after going through the saturable absorber back and forth inside the resonator. Whereas for intracavity Raman lasers, first Stokes line intensity grow nonlinearly with the pumping beam intensity. The lucky spike whose intensity surpasses the SRS threshold first, experiences larger Raman gain, and grow into pulse profile after going through the Raman medium back and forth. In a word, these two passive mode-locking ways realize pulse choosing by using the resonator net gain.

For intracavity Raman lasers, the intensity fluctuation of the fundamental enhances the discrimination ability of the pulses, which is preferable for the self-mode locking of the first Stokes laser. The numerical results show that the self-mode-locking process of the intracavity Raman laser is closely related to the phonon lifetime of the Raman medium and the modulation depth of the fundamental laser, which is associated with the length of the resonator and the transverse relaxation time of the laser medium. With the shorter transverse relaxation time of laser medium, shorter resonator length, and shorter phonon lifetime of Raman medium, more perfect mode-locked pulses of Stokes line can be obtained.

Calculated with the relative data listed in Table I, numerical results show temporal profiles of the fundamental and Stokes pulses from the LD end-pumped AO Q-switched $Nd:YAG/SrWO_4$ intracavity Raman laser in Fig. 11, and the resonator length is 15 cm [Fig. 11(a)], and 40 cm [Fig. 11(b)], respectively. From the numerical and experimental results depicted in Figs. 5, 6, and 11, it is shown that longer resonator length results in deeper intensity modulation of the intracavity fundamental laser, enhances the discrimination ability of the Stokes pulses, and perfect mode-locked pulses of the Stokes line are produced.

In Figs. 12 and 13, numerical results show the temporal profiles of the fundamental and Stokes pulses from the intracavity Raman laser, the phonon lifetime is $T_3=25\times10^{-12}$ s and $T_3=10\times10^{-12}$ s in Figs. 12 and 13, respectively. The resonator length is 10 cm, and the transversal dephasing time of the laser crystal is $T_2=1\times10^{-10}$ s. It can be seen that shorter phonon lifetime of the Raman laser is preferable for self-mode locking. Numerical results in Figs. 14 is the same as Fig. 12 except for the transversal dephasing time of laser crystal is $T_2=7\times10^{-11}$ s. It can be seen that

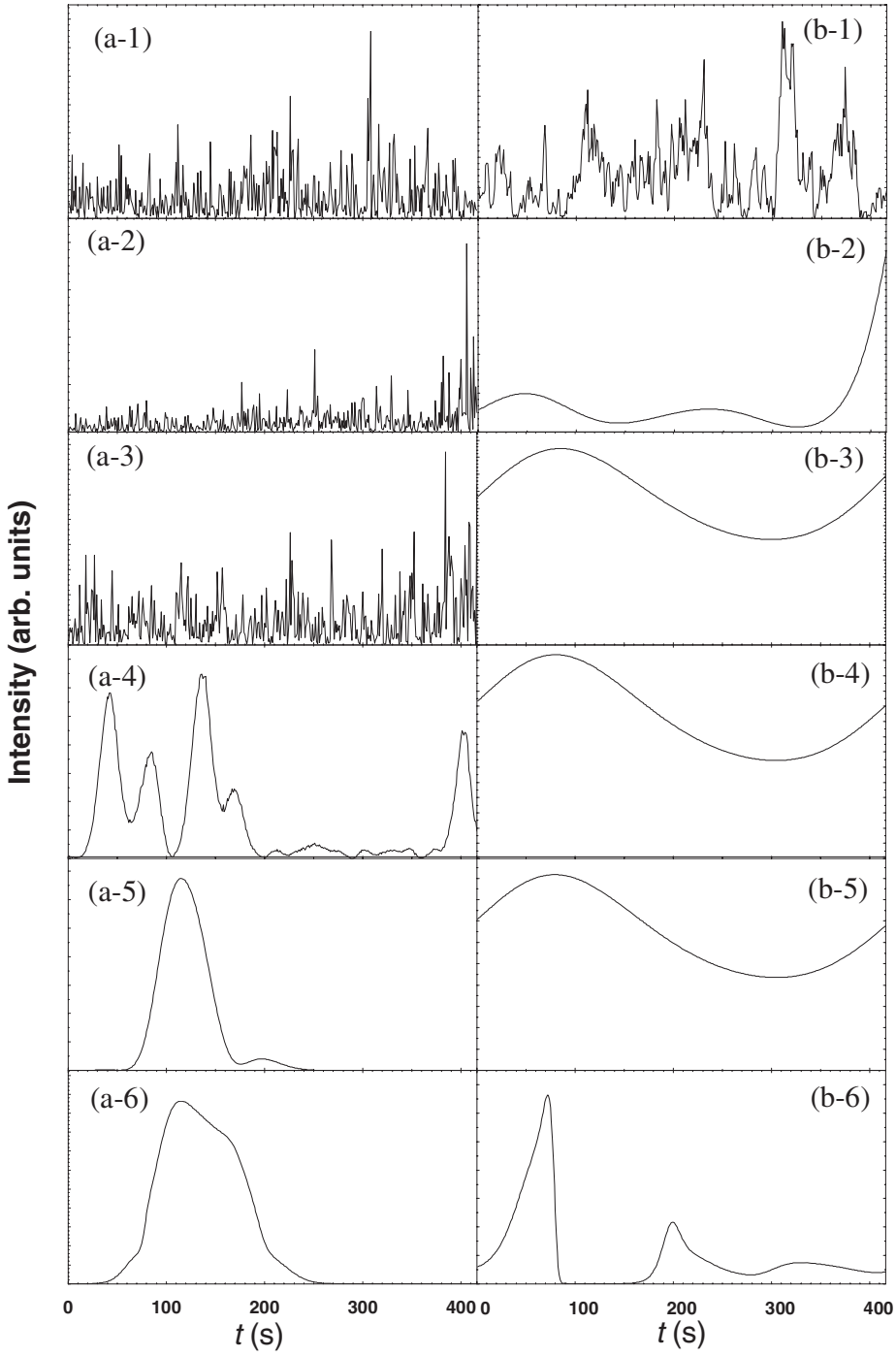

FIG. 10. Numerical results show evolution of the fundamental and Stokes intensity from spontaneous emission noise for LD end-pumped AO Q-switched $Nd:YAG/SrWO_4$ intracavity Raman laser. Each picture represents output intensity over a single round-trip period of 3.79 ns. The Stokes output intensity is shown in (a-1)–(a-6) with the round-trip number of 4, 14, 35, 38, 48, and 58, respectively, and the corresponding fundamental output intensity is shown in (b-1)–(b-6).

shorter transverse relaxation time of the laser medium will bring deeper modulation for the fundamental laser, and lead to better self-mode locking of the intracavity Raman laser.

From the numerical calculation, it is found there is a statistical factor in the production of well-defined Raman self-mode-locked pulses. In order to test the effect on the final pulse structure of the spontaneous Raman scattering, the calculation was carried out with a different set of spontaneous Raman scattering initials. Due to the quantum statistical nature of the spontaneous Raman scattering, there is large pulse-to-pulse variations. Though comparison of the results of different laser parameters, it is shown statistics are better for the production of well-defined Raman self-mode-locked pulses when the laser is operated near the threshold of the first Stokes line than when it is operated well above, which is similar to the way of the passive mode-locked lasers.

V. CONCLUSION

In this paper, based on the wave equation and SRS material equations, and with the phonon lifetime and backward Raman scattering considered, the traveling-wave (TW) equations of the SRS process were deduced in detail. Spontaneous Raman scattering was simulated by including the sto-

TABLE I. Parameters for theoretical simulations.

	Parameter	Value
ω_R	Raman shift of YVO_4 crystal	921 cm^{-1}
g	Raman gain coefficient of $SrWO_4$ crystal (at 1064 nm)	5 cm/GW
T_{S2}	Phonon dephasing time of $SrWO_4$ crystal	4 ps
n_2	Refractive index of $SrWO_4$ crystal	2.13
σ	Stimulated emission cross section of Nd:YAG crystal	6.5×10^{-19} cm^2
τ	Stimulated radiation lifetime of Nd:YAG crystal	230 μs
n_1	Refractive index of Nd:YAG crystal	1.82
l	Length of Nd:YAG crystal	10 mm
l_R	Length of $SrWO_4$ crystal	49 mm
L_L	Intrinsic loss of the resonator at the fundamental	0.08
L_R	Intrinsic loss of the resonator at the first Stokes line	0.08
L	Geometrical resonator length	40 cm
R_{L2}	Output coupling rate at the fundamental	0.01
R_{R2}	Output coupling rate at the Stokes line	0.23

chastic shot-noise sources in the phonon wave equations. The numerical methods of second-order accuracy are deduced for the TW equations of SRS process.

In this paper, the TW method is adopted to simulate the evolution of the fundamental light inside the actively Q-switched laser. The numerical results show that the output Q-switched pulse exhibits the periodical self-modulation, and the modulation period is equal to the round-trip transit time of the resonator. From the calculation results, it is found that shorter transverse relaxation time and longer resonator leads to deeper self-modulation of the fundamental laser. Self-modulation effect of the actively Q-switched laser was also studied experimentally, and the theoretical results were in good agreement with the experimental ones.

The evolutions of first Stokes line from spontaneous Raman scattering were simulated numerically, and the numerical results showed the self-mode-locking effect of the first Stokes line. From the numerical modeling, it is found that the mechanism of the self-mode locking of the intracavity Raman laser is similar to that of the passively saturable absorbers. The first Stokes intensity grow exponentially with the pumping beam intensity. In the spontaneous Raman scattering emission, the lucky spike whose intensity surpasses the SRS threshold experiences larger Raman gain, and grow

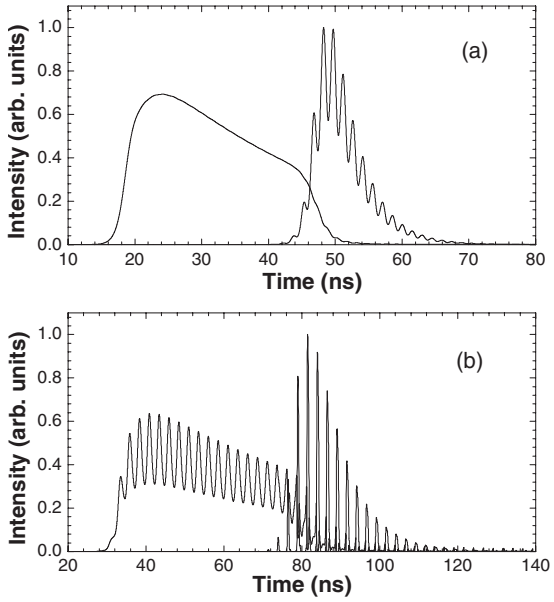

FIG. 11. Numerical results show the temporal profiles of the fundamental and Stokes pulses from the LD end-pumped AO Q-switched Nd:YAG/$SrWO_4$ intracavity Raman laser. For convenience, the intensity of the fundamental pulse has been multiplexed by a factor of 10 (a) and 30 (b). The resonator length is 15 cm (a) and 40 cm (b).

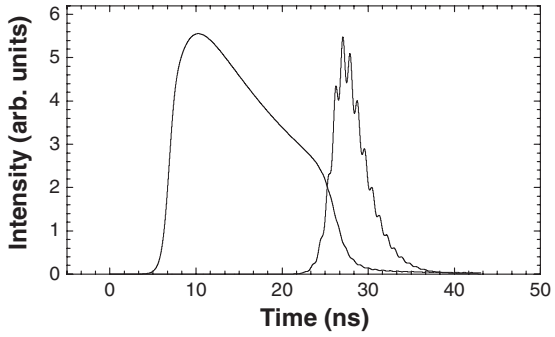

FIG. 12. Numerical results show the temporal profiles of the fundamental and Stokes pulses from the intracavtiy Raman laser. The resonator length is 10 cm. The transversal dephasing time of the laser crystal is $T_{L2}=1\times10^{-10}$ s, and the phonon lifetime is $T_{S2}=25\times10^{-12}$ s. For the convenience, the intensity of the fundamental pulse shown in the figure has been multiplexed by a factor of 30.

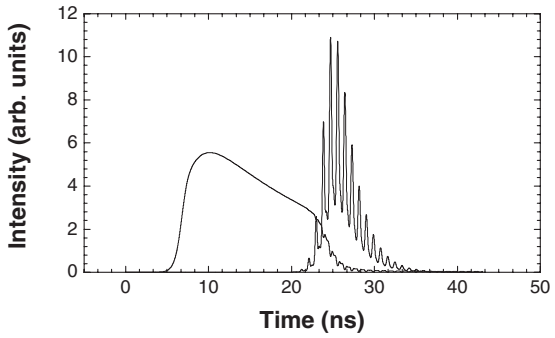

FIG. 13. Same as Fig. 11 except that the phonon lifetime is $T_{S2}=10\times10^{-12}$ s.

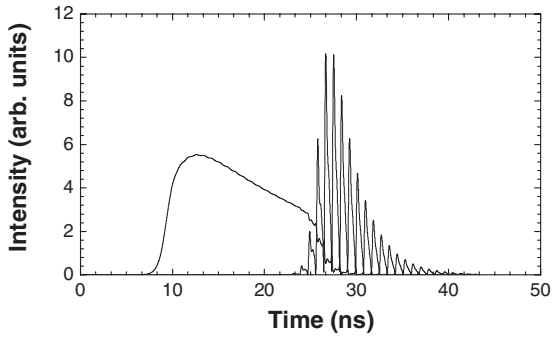

FIG. 14. Same as Fig. 11 except that the transversal dephasing time of the laser crystal is $T_{L2}=7\times10^{-11}$ s.

rapidly into pulse profile after going through the Raman medium back and forth inside the resonator. In a word, these two passive mode-locking ways realize pulse choosing by the resonator net gain. The numerical results show that shorter phonon lifetime of Raman medium, shorter transverse relaxation time of laser medium, and longer resonator are preferable for perfect mode-locking of the intracavity Raman laser.

From the numerical calculation, it is found there is a statistical factor in the production of well-defined Raman self-mode-locked pulses due to the quantum statistical nature of the spontaneous Raman scattering. The results show statistics are better for the production of well-defined Raman self-mode-locked pulses when the laser is operated near the threshold of the first Stokes line than when it is operated well above.

ACKNOWLEDGMENTS

This research is partly supported by the National Natural Science Foundation of China (Contact No. 60277023 and No. 60277023). This work is also supported by the Research Foundation for the Young Scientists of Yantai University and Research Foundation for Doctors of Yantai University.

[1] D. J. Kuizenga, D. W. Phillion, T. Lund, and A. E. Siegman, Opt. Commun. **9**, 221 (1973).
[2] L. Misoguti, C. R. Mendonca, and S. C. Zilio, Appl. Phys. Lett. **74**, 1531 (1999).
[3] R. V. Johnson and J. H. Marburger, Phys. Rev. A **4**, 1175 (1971).
[4] G. I. Kachen and W. H. Lowdermilk, Phys. Rev. A **16**, 1657 (1977).
[5] P. Christov and I. V. Tomov, Opt. Quantum Electron. **17**, 207 (1985).
[6] Y. B. Band, J. R. Ackerhalt, J. S. Krasinski, and D. F. Heller, IEEE J. Quantum Electron. **25**, 208 (1989).
[7] J. R. Ackerhalt, Y. B. Band, J. S. Krasinski, and D. F. Heller, Opt. Lett. **13**, 646 (1988).
[8] J. Simons, H. Pask, P. Dekker, and J. Piper, Opt. Commun. **229**, 305 (2004).
[9] H. M. Pask and J. A. Piper, IEEE J. Quantum Electron. **36**, 949 (2000).
[10] H. M. Pask and J. A. Piper, Opt. Commun. **148**, 285 (1998).
[11] H. Ogilvy, H. M. Pask, J. A. Piper, and T. Omatsu, Opt. Commun. **242**, 575 (2004).
[12] J. A. Fleck, Jr., Phys. Rev. Lett. **21**, 131 (1968).
[13] J. A. Fleck, Jr., Appl. Phys. Lett. **12**, 178 (1968).
[14] J. A. Fleck, Jr., Phys. Rev. B **1**, 84 (1970).
[15] J. A. Giordmaine and M. Maier, Phys. Rev. **144**, 676 (1966).
[16] P. G. Kryukov and V. S. Letokhov, IEEE J. Quantum Electron. **8**, 766 (1972).
[17] H. A. Haus, J. Appl. Phys. **46**, 3049 (1975).
[18] M. Maier, W. Kaiser, and J. A. Giordmaine, Phys. Rev. **177**, 580 (1969).
[19] Y. R. Shen and N. Bloembergen, Phys. Rev. **137**, 1787 (1965).
[20] C. S. Wang, Phys. Rev. **182**, 482 (1969).
[21] J. A. Giordmaine and M. Maier, Phys. Rev. **144**, 676 (1966).
[22] H. M. Pask and J. A. Piper, Opt. Commun. **148**, 285 (1998).
[23] K. A. Stankov and G. Marowsky, Appl. Phys. B: Lasers Opt. **61**, 213 (1995).